Longitudinal noninvasive PET-based β cell mass estimates in a spontaneous diabetes rat model

Fabiola Souza, … , Ronald Van Heertum, Paul E. Harris

Research Article   **Metabolism**

Diabetes results from an absolute or relative reduction in pancreatic β cell mass (BCM) leading to insufficient insulin secretion and hyperglycemia. Measurement of insulin secretory capacity is currently used as a surrogate measure of BCM. However, serum insulin concentrations provide an imprecise index of BCM, and no reliable noninvasive measure of BCM is currently available. Type 2 vesicular monoamine transporters (VMAT2) are expressed in human islet β cells, as well as in tissues of the CNS. [11C]Dihydrotetrabenazine ([11C]DTBZ) binds specifically to VMAT2 and is a radioligand currently used in clinical imaging of the brain. Here we report the use of [11C]DTBZ to estimate BCM in a rodent model of spontaneous type 1 diabetes (the BB-DP rat). In longitudinal PET studies of the BB-DP rat, we found a significant decline in pancreatic uptake of [11C]DTBZ that anticipated the loss of glycemic control. Based on comparison of standardized uptake values (SUVs) of [11C]DTBZ and blood glucose concentrations, loss of more than 65% of the original SUV correlated significantly with the development of persistent hyperglycemia. These studies suggest that PET-based quantitation of VMAT2 receptors provides a noninvasive measurement of BCM that could be used to study the pathogenesis of diabetes and to monitor therapeutic interventions.

Find the latest version:

https://jci.me/27645/pdf

Longitudinal noninvasive PET-based β cell mass estimates in a spontaneous diabetes rat model

Fabiola Souza,[1] Norman Simpson,[2] Anthony Raffo,[1] Chitra Saxena,[2] Antonella Maffei,[3] Mark Hardy,[4] Michael Kilbourn,[5] Robin Goland,[6] Rudolph Leibel,[6] J. John Mann,[7] Ronald Van Heertum,[2] and Paul E. Harris[1,3]

[1]Department of Medicine and [2]Department of Radiology, Columbia University Medical Center, New York, New York, USA. [3]Institute of Genetics and Biophysics "Adriano Buzzati-Traverso," Consiglio Nazionale delle Ricerche, Naples, Italy. [4]Department of Surgery, Columbia University Medical Center, New York, New York, USA. [5]Department of Radiology, University of Michigan, Ann Arbor, Michigan, USA. [6]Naomi Berrie Diabetes Center and [7]Department of Psychiatry, Columbia University Medical Center, New York, New York, USA.

Diabetes results from an absolute or relative reduction in pancreatic β cell mass (BCM) leading to insufficient insulin secretion and hyperglycemia. Measurement of insulin secretory capacity is currently used as a surrogate measure of BCM. However, serum insulin concentrations provide an imprecise index of BCM, and no reliable noninvasive measure of BCM is currently available. Type 2 vesicular monoamine transporters (VMAT2) are expressed in human islet β cells, as well as in tissues of the CNS. [11C]Dihydrotetrabenazine ([11C]DTBZ) binds specifically to VMAT2 and is a radioligand currently used in clinical imaging of the brain. Here we report the use of [11C]DTBZ to estimate BCM in a rodent model of spontaneous type 1 diabetes (the BB-DP rat). In longitudinal PET studies of the BB-DP rat, we found a significant decline in pancreatic uptake of [11C]DTBZ that anticipated the loss of glycemic control. Based on comparison of standardized uptake values (SUVs) of [11C]DTBZ and blood glucose concentrations, loss of more than 65% of the original SUV correlated significantly with the development of persistent hyperglycemia. These studies suggest that PET-based quantitation of VMAT2 receptors provides a noninvasive measurement of BCM that could be used to study the pathogenesis of diabetes and to monitor therapeutic interventions.

Introduction

The natural history of type 1 diabetes is progression to complete loss of insulin secretory capacity and dependence on exogenous insulin for survival. As assessed by measurements of islet cell autoantibodies, there is a variable preclinical period during which the immunologic assault is ongoing, but sufficient insulin is secreted for preservation of euglycemia (1). Hyperglycemia occurs in type 1 diabetes when insulin secretion becomes inadequate. Patients with type 2 diabetes display a relative or absolute loss of insulin production as well (2). Early in the course of type 2 diabetes, as individuals become insulin resistant, circulating insulin concentrations increase. Diabetes occurs when insulin production, and presumably β cell mass (BCM), can no longer compensate for the increased need for insulin. Endogenous insulin secretion declines progressively in type 2 diabetes, probably reflecting, in part, the loss of BCM (3). There is, at present, no in vivo measure of BCM that would allow estimation of the relative contributions of functional versus anatomical defects in insulin secretion to these types of diabetes. The ability to quantify BCM changes during the early progression of diabetes would provide important biological insights and facilitate aspects of diagnosis and therapy, including islet transplantation.

The critical BCM needed to avert diabetes depends on the size of the individual, the degree of insulin resistance, and the intercurrent metabolic stress. The relationship between BCM and glucose homeostasis has been characterized in many studies using several species and a number of different approaches to measuring β cell function (4). In the Göttingen minipig, fasting and postprandial plasma glucose concentrations are affected only when BCM is reduced to approximately 5 mg/kg body mass versus the normal value of 20 mg/kg (5). The approximately 75% reduction of BCM resulting in fasting hyperglycemia is consistent with a previous study in which an approximately 60% reduction in BCM resulted in fasting hyperglycemia in minipigs (6, 7). Similar studies in baboons have shown that a 50–60% reduction of BCM results in deranged glucose homeostasis (8), whereas in both humans (9–11) and rodents (12, 13) different experimental approaches suggest that a 70–90% reduction of BCM may be required to produce fasting hyperglycemia. For example, BCM was reduced by 42% in 13-week-old nondiabetic NOD mice, and by 73% in 18-week-old diabetic NOD mice (4). In BioBreeding diabetes-prone/Wor (BB-DP) rats, pancreatic BCM was reduced by 75% on the first day of overt autoimmune diabetes (13). Most likely, these minor differences in estimates of critical BCM are due to species-specific differences, small sample sizes, and/or the likely variability in β cell function at very low BCM (7).

Imaging of the endocrine pancreas has been described in several studies. Fluorine-18 4-fluorobenzyltrozamicol binds to the vesicular acetylcholine transporter that is present on presynaptic vesicles in the neurons innervating the pancreas and can be used to image the body of the pancreas (14). Similarly, taking

---

Table 1
In vivo biodistribution of radiolabeled [11C]DTBZ

| | % Injected dose per gram[A] | | | | | | | |
| | 2 min | | 15 min | | 30 min | | 60 min | |
Tissue	Mean	SD	Mean	SD	Mean	SD	Mean	SD
Brain	1.058	0.098	0.754	0.036	0.486	0.067	0.448	0.021
Eyeballs	0.383	0.045	0.239	0.019	0.228	0.069	0.192	0.029
Heart	1.411	0.228	0.568	0.014	0.882	0.079	0.387	0.026
Lung	1.286	0.339	0.738	0.114	0.585	0.033	0.514	0.059
Liver	2.044	0.297	3.572	0.477	3.382	0.574	3.603	0.282
Pancreas	2.268	0.342	5.652	1.109	6.205	1.933	7.112	1.254
Spleen	1.270	0.247	1.488	0.187	0.978	0.266	0.851	0.086
Adrenal	2.403	0.282	1.114	0.073	1.110	0.372	0.677	0.100
Kidney	4.082	0.294	1.567	0.097	2.604	0.190	1.079	0.088
Adipose	0.289	0.067	0.480	0.079	0.480	0.063	0.319	0.071
Stomach	0.934	0.186	2.000	0.475	1.066	0.418	1.085	0.155
Contents of stomach	0.139	0.105	1.207	0.668	0.836	0.625	2.907	1.745
SI	1.297	0.243	1.424	0.109	1.647	0.337	1.276	0.231
Contents of SI	0.608	0.289	0.513	0.202	1.384	1.069	0.563	0.095
Cecum	1.075	0.339	0.645	0.109	0.648	0.176	0.442	0.102
Contents of cecum	0.175	0.147	0.110	0.024	0.304	0.210	0.149	0.029
LI	1.060	0.182	1.002	0.125	0.878	0.202	0.813	0.151
Contents of LI	0.158	0.052	0.234	0.133	0.338	0.238	0.214	0.076
Ovary	1.519	0.107	1.051	0.050	4.746	4.091	0.653	0.014
Uterus	0.913	0.021	0.718	0.066	0.467	0.222	0.489	0.052
Muscle	0.393	0.215	0.327	0.028	0.431	0.144	0.209	0.023
Bone	0.455	0.056	0.555	0.039	2.792	3.895	0.368	0.089
Blood	0.393	0.053	0.229	0.007	0.180	0.045	0.158	0.005
Testes	0.339	0.002	0.569	0.024	0.306	0.246	0.867	0.062
Urine	0.173	0.000	9.738	4.030	6.921	6.215	16.613	1.271

[A]The reported data are corrected for the decay of 11C. SI, small intestine; LI, large intestine.

advantage of the bicarbonate and/or organic anion transporters expressed by pancreatic acinar cells, [11C]acetate has been used to visualize the exocrine pancreas (15, 16). Fourteen months after transplantation, cadaveric islets induce peri-islet fat deposits in the liver parenchyma that are visible by chemical shift gradient–echo magnetic resonance imaging (17).

Using β cell–specific anti-IC2 mAb, modified with a radioisotope chelator, Moore et al. studied normal and type 1 diabetic rodent pancreata by radioimmunoscintigraphy. Mice with streptozotocin-induced diabetes showed a 50% loss of BCM and significantly lower accumulation of the probe than control animals (18). It is unclear whether the method has clinical promise, as imaging was performed on pancreata ex vivo. Radioimmunoscintigraphy with anti-ganglioside mAbs has been less promising because of low specificity (19).

The in vivo uptake of 6-deoxy-6-[125I]iodo-D-glucose by pancreata of normal versus streptozotocin-injected rats has been compared. Although islets and acinar tissue showed differential uptake of the

Table 2
BB-DP rat PET scan and IPGTT study protocol

| | Age | | | | | | | | | | | | | | | | | | | | | | | |
| | 7 Weeks | | | | 8 Weeks | | | | 9 Weeks | | | | 10 Weeks | | | | 11 Weeks | | | | 12 Weeks | | | |
Animal ID	T	W	Th	F	T	W	Th	F	T	W	Th	F	T	W	Th	F	T	W	Th	F	T	W	Th	F
A	G[A]	P	G	–	G	–	G	P	G	–	G	–	G	–	–	G	G	P	G	–	G	**P**	G	–
B	G	P	G	–	G	–	G	P	G	–	G	–	G	–	–	G	G	P	G	–	G	**P**	G	–
C	G	P	G	–	G	–	G	P	G	–	G	–	G	–	–	G	G	P	G	–	G	**P**	G	–
D	G	P	G	–	G	–	G	–	G	–	G	P	G	–	–	G	G	–	G	P	–	–	–	–
E	G	–	G	P	G	–	G	–	G	–	G	P	G	–	–	G	G	–	G	**P**	–	–	–	–
F	G	–	G	P	G	–	G	–	G	–	G	P	G	–	–	G	G	–	G	–	G	–	G	**P**
G	G	–	G	P	G	–	G	–	G	–	G	P	G	–	–	G	G	–	G	–	G	–	G	**P**

[A]The frequency of IPGTT is shown (letter G) in relation to the frequency of PET scans using [11C]DTBZ (letter P) and age of the BB-DP rats. Four-hour-fasting whole-blood (tail vein) glucose concentrations were determined daily. The use of a boldface letter indicates that the animal was diabetic (at least 4 measurements of fasting blood glucose ≥ 300 mg/dl over 4 days) at the time of the PET scan. T, W, Th, and F indicate days of the week.
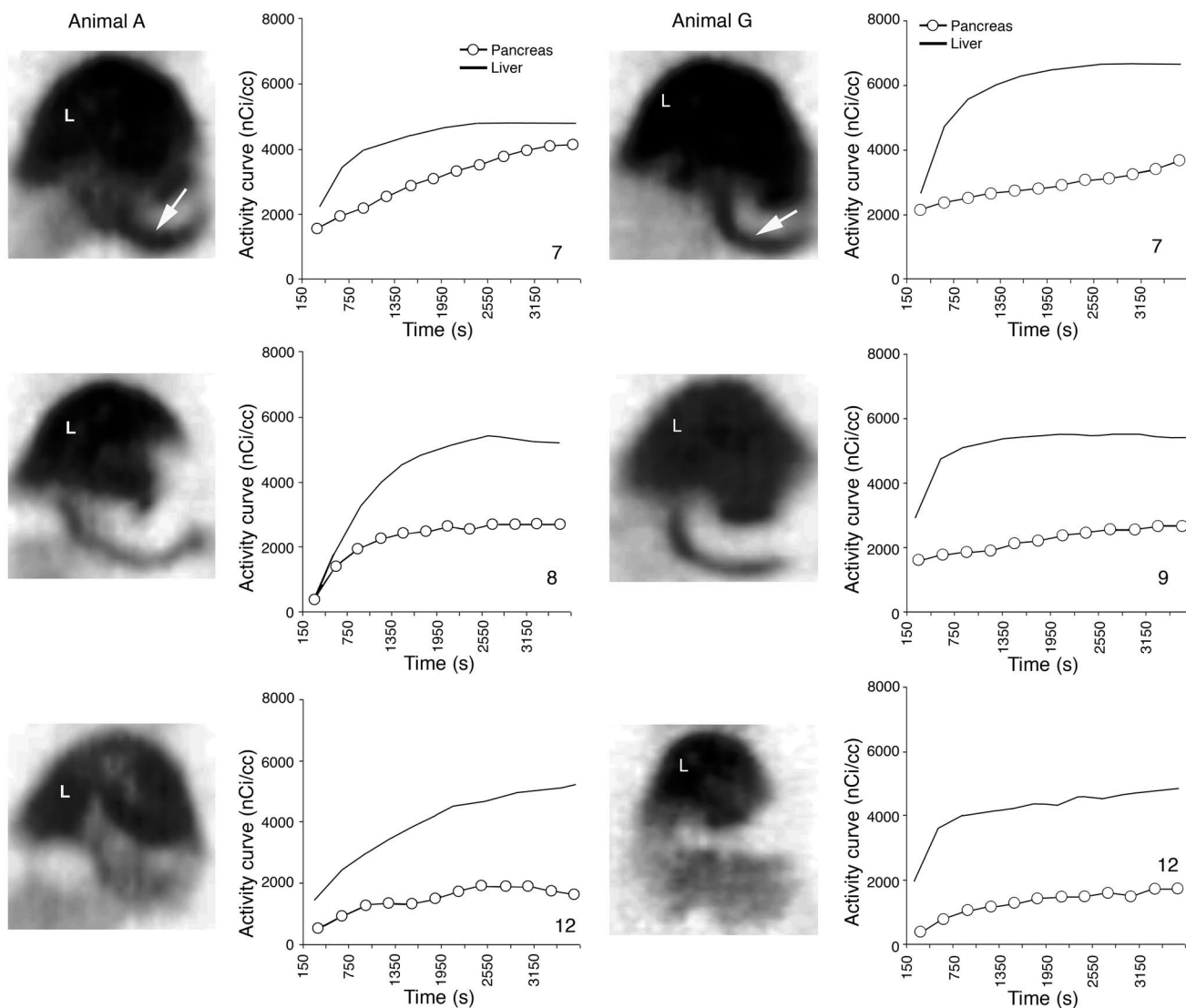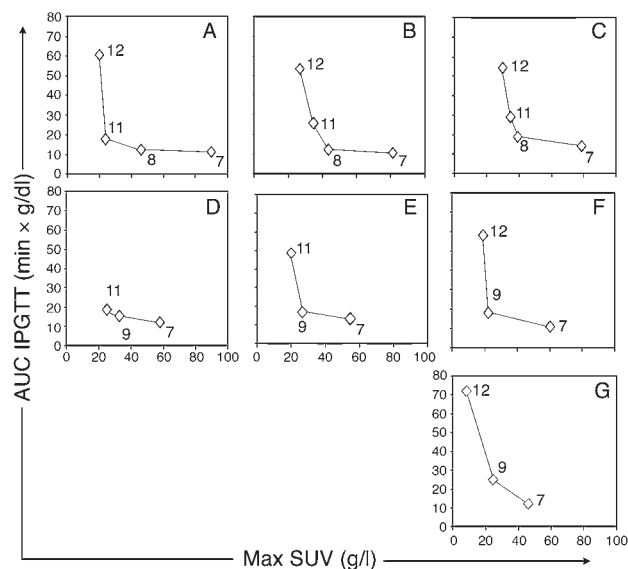
Figure 1
Representative reconstructed serial PET images of coronal abdominal planes of BB-DP rats during progression of autoimmune diabetes. The bodies of the pancreata of animals A and G are identified by large arrows; the livers are identified by the letter L. Approximately 300 μCi of (+)-α-[^{11}C]DTBZ was used for imaging. Euglycemic male rats were imaged to establish a baseline at approximately 7 weeks of age; these animals were reimaged 2 or 3 times during the following 5 weeks. Whole-venous-blood glucose concentrations of 7-week-old animals fasted for 4 hours ranged from 90 to 135 mg/dl. Reconstructed images represent the summed data of the entire 1-hour-long scanning period. Display ranges of images are not equivalent. Quantitation of activity within pancreas and liver regions of interest during the scan period is shown in the time-activity curves in the panels at the right. The age of the animal in weeks appears in the lower right corner. The average activity of [^{11}C]DTBZ in nCi/cc of tissue within the liver or pancreatic regions of interest versus the duration of the PET scan in seconds is plotted on the ordinates and abscissae, respectively. Solid lines represent activity in the liver, and open circles represent activity in pancreas regions of interest.

radioligand, and pancreata depleted of β cells showed decreased uptake, the clinical utility of this approach is unclear because of the low tissue specificity of binding of the radioligand, and high uptake in the liver (20). Pancreatic uptake of [2-(14)C]alloxan, targeting the GLUT2 transporter, has been studied in normal and streptozotocin-treated rodents. Greater uptake of the radiotracer in normal versus diabetic pancreata was demonstrated (21). Dithizone and sulfonylurea receptor ligands (e.g., ^{3}H-glibenclamide) have been studied as possible imaging agents but show broad tissue distributions of uptake (22–24).

The β cells of the pancreas and neurons share expression of a large number of genes and display some functional similarities (25–27). Vesicular monoamine transporter type 2 (VMAT2) is expressed at dopamine nerve terminals in the CNS and by β cells but is absent from the exocrine pancreas and many other intra-abdominal tissues (28). A specific ligand for VMAT2, dihydrotetrabenazine (DTBZ), is already in clinical use for PET imaging of the CNS (29). We studied the binding of [^{3}H]DTBZ to total membrane fractions prepared from purified human islets and purified exocrine pancreas tissue. [^{3}H]DTBZ bound specifically to islet mem-

measurements (usually made the day before the scan) were significantly correlated with pancreatic [11C]DTBZ uptake (i.e., max SUV) by a hyperbolic function ($P = 0.005$). The curve obtained had the following characteristics: (a) at infinitely high max SUVs, the curve became asymptotic to the line $y = 10$ min × g/dl, consistent with the blood glucose concentration of a euglycemic animal at the beginning of the study (i.e., 120 min × 0.083 g/dl); and (b) at infinite values of AUC IPGTT, the max SUV index approached the line approximated by $x = 8$ g/l, consistent with the range of max SUVs obtained from the abdominal wall and kidney, where VMAT2 is not expressed (e.g., following complete β cell destruction in the pancreas).

We also determined whether there was a correspondence between max SUV and BCM as determined by histomorphometry. At the end of the study period, pancreata from diabetic rats were harvested, processed for sectioning, and stained with anti-insulin antibodies. Since max SUV is derived from a density measurement (i.e., amount of [11C]DTBZ per cubic centimeter tissue), we determined an area density measurement for the BCM expressed as percentage β cell fraction (i.e., β cell area relative to total pancreas area). To obtain max SUV and percentage β cell fraction measurements at an intermediate point in the development of diabetes by BB-DP rats, we studied 2 additional male animals. In those 6- to 7-week-old animals, we first confirmed normal glucose tolerance with an IPGTT. Twice-weekly IPGTT testing was then performed until the animals converted to an abnormal IPGTT (age approximately 8–9 weeks), at which point the animals were imaged and sacrificed and the pancreata were processed for immunohistochemistry. The max SUV and percentage β cell fraction value from these 2 animals are shown

branes, but not to membranes from the exocrine pancreas (28). By immunohistochemistry, anti-VMAT2 and insulin immunoreactivity were colocalized in islet β cells; VMAT2 was not present in the other endocrine cells of the islets or the exocrine pancreas (30–32). In the present study, we assessed use of [11C]DTBZ to image the endocrine pancreas in vivo, and to monitor β cell loss in a rodent model of progressive autoimmune diabetes (the BB-DP rat) (see review refs. 33–35). We found that changes in BCM can be readily estimated by serial PET using [11C]DTBZ.

Results

The in vivo biodistribution of [11C]DTBZ uptake in the rat reflects the tissue distribution of VMAT2 expression. In feasibility studies, the biodistribution of [11C]DTBZ in rats was obtained as previously reported by Kilbourn and colleagues (36). The in vivo biodistribution of DTBZ is higher in the pancreas than in many other abdominal organs (Table 1).

Longitudinal PET studies in the BB-DP rat show continuous loss of [11C]DTBZ uptake in the pancreas during progression toward overt diabetes. Serial PET scans were performed on 7 BB-DP male rats. Each animal was imaged once at a baseline of 7 weeks of age; this was followed by an additional 2 or 3 scans in the subsequent 5 weeks (Table 2). At baseline, all the animals were euglycemic (range 90–135 mg/dl), had detectable serum insulin concentrations (>1.0 ng/ml), and had values less than 14 min × g/dl for the area under the curve of the intraperitoneal glucose tolerance test (AUC IPGTT). A second PET scan was performed during weeks 8–9 of age while the majority of animals were still euglycemic. However, maximum standardized uptake values (max SUVs) at 8–9 weeks of age were only approximately 50% of the baseline values ($P < 0.005$). Max SUVs continued to decline and, at weeks 11 and 12, were significantly lower than the max SUVs measured at weeks 8 and 9 ($P < 0.02$) (Figures 1 and 2). In one instance, animal G, on the first PET scan at 6 weeks, we were unable to obtain the maximal uptake of [11C]DTBZ in the pancreas. The presented max SUV in this instance probably represents an underestimate.

Max SUV and age were correlated ($r^2 = 0.58$), suggesting a relationship between max SUV and disease progression. In this study, AUC IPGTT values provided an index of glycemic control. These

Table 3
Correlation of histomorphometric measurements of β cell area, max SUV, and AUC IPGTT

Animal ID	% β Cell area	Max SUV (min × g/dl)	AUC IPGTT (g/l)
G[A]	0.10	8	72
C	0.22	27	53
B	0.23	22	54
H[B]	1.14	60	18
I	1.28	45[C]	25
J	1.45		11
K	1.51		113

[A]The β cell area density measurements were performed at the end of the study in 3 BB-DP rats (animals G, B, and C). [B]Four additional animals (H–K) were studied for β cell area density: 2 animals imaged after development of an abnormal IPGTT (H and I), and 2 euglycemic animals at 6 weeks of age (J and K). [C]The percentage β cell fraction and max SUV were linearly correlated ($n = 5$, $r^2 = 0.81$, $P = 0.04$). The percentage β cell fraction and AUC IPGTT were well correlated through either a hyperbolic or a linear function ($n = 7$, $r^2 > 0.80$, $P < 0.005$).

Table 4

Quantitation of VMAT2 mRNA in pancreata of euglycemic and diabetic BB rats

Age	AUC IPGTT[A] (min × g/dl)	Relative accumulation of VMAT2-specific mRNA			
6–7 Wk	<11 (Euglycemic)	1.0[B]	1.3	3.7	1.7
			Mean = 1.9		
>10 Wk	>33 (Diabetic)	0.051	0.31	0.0084	0.12
			Mean = 0.16[C]		

[A]AUC IPGTT is an index of glycemic control calculated from the averages of the area under the curve of intraperitoneal glucose tolerance tests measured in min × g/dl. [B]The normalized levels of VMAT2 transcripts for each animal studied are relative to 1 of the control samples taken from euglycemic BB rats at 6–7 weeks of age. [C]The relative level of transcripts at >10 weeks of age was significantly different ($P < 0.05$) from the value at 6–7 weeks. The P value was determined using 2-tailed Student's t test.

in Table 3 (animals H and I). We also determined the percentage β cell fraction in normal pancreata from 2 euglycemic 7-week-old BB-DP rats as additional referents (Table 3, animals J and K).

VMAT2 expression within the total pancreas of euglycemic and diabetic BB-DP rats was measured. Both immunohistochemistry (data not shown) and real-time PCR measurements using total RNA prepared from whole pancreata showed significantly reduced expression of VMAT2 in diabetic pancreata relative to euglycemic controls (Table 4).

Changes in [11C]DTBZ uptake in the pancreas are significantly associated with loss of glycemic control. Using longitudinal measurements of max SUV, IPGTT, and the matched 4-hour fasting blood glucose concentrations, we assessed the statistical strength of the associations between changes in max SUV of [11C]DTBZ activity in the pancreas and the presence of an abnormal IPGTT and persistent hyperglycemia. As there was variation among animals in the initial max SUVs, we calculated the percentage residual SUV for each animal, as an estimate of residual BCM. This index was calculated as follows: *percentage residual SUV* = $[1 - (\text{max SUV}_i - \text{max SUV}_t/\text{max SUV}_i)] \times 100$, where max SUV$_t$ is the max SUV at 8–12 weeks and max SUV$_i$ is the max SUV at baseline (7 weeks).

Threshold values for percentage residual SUV and AUC IPGTT were selected from receiver operator characteristic (ROC) curves for maximum specificity and sensitivity of detection of persistent hyperglycemia (AUC ROC > 0.99; 95% confidence interval = 0.84–0.99). A reduction of max SUV to less than 35% of its original value was significantly associated ($P = 0.024$) with the presence of abnormal glucose tolerance (AUC IPGTT > 29 min × g/dl) and persistent hyperglycemia (at least 4 measurements of fasting blood glucose ≥ 300 mg/dl) by χ^2 analysis (Table 5).

Discussion

Our data indicate that longitudinal PET studies, using [11C]DTBZ to target β cells of the endocrine pancreas, can provide estimates of BCM that may be useful for the study and management of diabetes. Although the threshold values need further confirmation, we show that a measurable decline in uptake of [11C]DTBZ by the pancreas anticipates the loss of glycemic control.

DTBZ selectively targets VMAT2 (37, 38); the neuropharmacology and neurofunctional anatomy of VMAT2 have been reviewed in detail (31, 39). Weihe and colleagues (30, 32), and our own data

(28), have shown that VMAT2 immunoreactivity colocalizes with insulin, or is coexpressed with other β cell markers, and is absent from human, rodent, and nonhuman primate islet cells stained with anti-glucagon, anti-somatostatin, and anti-pancreatic polypeptide antibodies. High levels of VMAT2 expression are limited to monoaminergic cell bodies of the CNS, chromaffin cells of the adrenal medulla, the oxyntic mucosa of the stomach, and β cells of the endocrine pancreas (28, 31). Our studies of the biodistribution of radiolabeled DTBZ reflect this pattern of expression. In preliminary studies with nonhuman primates, we found that [11C]DTBZ uptake in the mucosa of the stomach and other organs did not interfere with uptake measurements in the pancreas (Figure 3 and data not shown). Progression to diabetes in the BB rat resulted in a global loss of VMAT2-specific mRNA expression within the pancreas, confirming immunohistochemistry experiments, and suggesting that serial measurements of [11C] uptake in the pancreas could be used to monitor changes in BCM.

Serial measurements of [11C]DTBZ uptake in the abdomens of BB-DP rats during progression to diabetes quantified radioligand uptake over time and allowed us to estimate VMAT2 transporter density in the anatomical space occupied by the pancreas. While there was variation among animals in the initial max SUVs, perhaps due to population differences in the initiation and rate of autoimmune destruction of β cells, we observed a progressive loss of transporter density as estimated by max SUV in each animal studied. The loss of transporter density anticipated — and later significantly correlated with — loss of glycemic control (i.e., AUC IPGTT). The paired AUC IPGTT value and max SUV obtained during the longitudinal study of 7 BB-DP rats fitted significantly to a hyperbolic function.

The β cell area densities during progression of diabetes measured by histomorphometry were in agreement with the findings of Tomita and Doull (40) and supported our inference that the max SUVs for the VMAT2 ligand [11C]DTBZ reflected BCM. The fractional decrements in max SUV are in agreement with previous estimates of threshold values of BCM that result in abnormal glucose tolerance and persistent hyperglycemia (5–13). Quantitative analysis of images reconstructed from the [11C]DTBZ PET scans performed at the end of the study, when most of the animals had developed overt diabetes, suggested that pancreatic VMAT2 was not completely ablated. Such "background" radioligand uptake

Table 5

Two-by-two contingency table analyses of changes in pancreatic [11C]DTBZ uptake and glycemic control in BB-DP rats

		AUC IPGTT > 29[B]		
		Yes	No	
% Residual	Yes	4	1	5
SUV[A] < 35	No	3	16	19
		7	17	24
		$\chi^2 = 5.097$, $P = 0.024$		

[A]The max SUVs were calculated as the highest activity measurement on the time-activity curve divided by the injected dose of [11C]DTBZ normalized to the total body weight of the animal at each time point studied. The percentage residual SUVs were calculated as the difference between max SUV at time t and the initial max SUV, divided by the initial max SUV, subtracted from 1 and multiplied by 100. [B]The cutoff values for percentage residual SUV and AUC IPGTT in relation to development of persistent hyperglycemia were determined using ROC statistics.
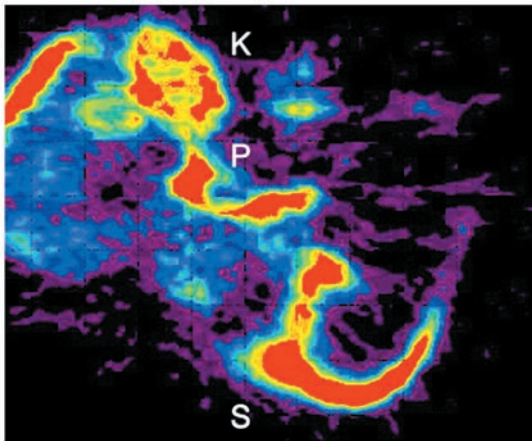
Figure 3
Transaxial reconstruction of a male-baboon abdominal dynamic PET scan with [11C]DTBZ. Kidney (K), pancreas (P), and stomach (S) are indicated in these summed early frames.

probably represents nonspecific uptake by pancreas tissue, residual β cells, and/or VMAT2 protein within nerve terminals of the pancreas. Recent studies by Mei et al. (41) also suggest that some of the initial decline in pancreatic [11C]DTBZ uptake may be due to autoimmune destruction of islet sympathetic nerve fibers.

At least 2 important questions are underscored but left unanswered by these studies: First, what purpose(s) do VMAT2 molecules serve in β cells? Purified islets (with little or no contamination from surrounding nervous tissue) contain monoamines such as epinephrine and dopamine (42), and at least some of the biosynthetic apparatus for these neurotransmitters can be detected in β cells (43). The role of these neurotransmitters as paracrine agents active in the control of secretory activity in islets is still largely speculative, but it has been shown that these neurotransmitters affect islet cell function (44–47). Second, is VMAT2 expression altered by the metabolic and immunologic consequences of the disease? Our studies have not addressed possibly confounding issues such as the effects of hyperglycemia and/or inflammation on the uptake of [11C]DTBZ in the pancreas regions of interest and BCM.

The coexpression of insulin and VMAT2 in human β cells is well documented, as is the safety of [11C]DTBZ in imaging the CNS in movement disorders (29, 48–50); this suggests that the approach described here could be useful in the evaluation of changes in BCM in human subjects in a variety of clinical and experimental circumstances.

Methods

Radioligands. The stereochemically resolved (+)-9-*O*-desmethyl-α-dihydrotetrabenazine precursor of [11C]DTBZ was obtained from ABX advanced biochemical compounds. Tritiated DTBZ was purchased from American Radiolabeled Chemicals Inc.

α[2³H]-DTBZ was labeled to a specific activity of 10–20 Ci/mmol. (+)-α-[11C]DTBZ was synthesized by [11C] methylation of the appropriate precursor, and the product was purified by HPLC (33, 51, 52). The purity of [11C]DTBZ preparations varied from 98.5% to 99.9% of the desired (+) product. Specific activities of carbon-11–labeled radiotracers were greater than 2,000 mCi/μmol at the end of synthesis.

Animals. All animal studies were reviewed and approved by the Institutional Animal Care and Use Committee (IACUC) at Columbia University Medical Center. All experiments were performed in accordance with the IACUC-approved procedures. All rodents were kept under specific pathogen–free conditions with standard light-dark cycles and were fed a regular diet and water ad libitum.

Age-matched (6-week-old) male BioBreeding diabetes-prone/Wor (BB-DP) rats were obtained from Biomedical Research Models Inc. BB-DP rats from the Biomedical Research Models Inc. colony have an average onset of hyperglycemia at 10 weeks of age (range 60–120 days), accompanied by hypoinsulinemia, weight loss, and ketonuria. The cumulative incidence of diabetes is greater than 93% in males. The schedule of the PET scans and the IPGTTs performed during the study is shown in Table 2. Sprague-Dawley rats used in the biodistribution studies were obtained from Taconic.

Biodistribution of radiolabeled DTBZ. Biodistribution studies of [11C]DTBZ in the Sprague-Dawley rats were performed as previously described (36). Briefly, rats were injected via the femoral vein with 150–650 μCi of [11C]DTBZ. Five animals per time point (3 females and 2 males) were sacrificed at 2, 15, 30, or 60 minutes after injection. Organs were removed, assayed for radioactivity in an automated gamma counter, and weighed. Data were calculated as percentage injected dose per gram organ weight.

Blood glucose and IPGTTs. Blood samples (5–10 μl) were collected from the tail veins of rats fasted for 4 hours. The whole-blood glucose levels of the rats were monitored daily using the glucose oxidase method with an Accu-Chek blood glucose monitoring system from Roche Diagnostics Corp. IPGTTs were performed in fasting unanesthetized animals as previously described (53) twice weekly from age 50 days. After baseline blood glucose measurements, animals received an i.p. injection of 2 g of glucose per kilogram body weight. Tail vein blood glucose concentrations were measured again 30, 60, 90, and 120 minutes later. Animals were considered diabetic when 4 consecutive daily fasting blood glucose values were above 300 mg/dl. Animals were considered to have an abnormal IPGTT response when 1 or more sequential blood glucose levels were greater than 200 mg/dl (53). The area under the IPGTT glucose concentration × time curve (AUC) was calculated by the trapezoidal rule for the IPGTT response (7).

Pancreas and islet histomorphometry. Rat pancreata were dissected, fixed in PBS/10% formalin, and embedded in paraffin. Five-micrometer-thick sections were deparaffinized and stained with H&E. Sections were also stained with guinea pig anti-bovine insulin antibodies from Sigma-Aldrich, and developed by standard indirect immunohistochemistry methods. Images from 5 slides per pancreas (sections taken at 500-μm intervals) were recorded with an optical Leica Microsystems DM E Microscope fitted with a PENTAX digital camera. Pancreatic tissue area, islet area, insulin-positive cell area, and islet number were determined by computer-assisted measurements using ImageJ software (version 1.34; NIH) that had been calibrated with a stage micrometer from Ted Pella Inc. (2 μm/division × 50 divisions). Percentage β cell fraction in the pancreas was calculated from the ratio of insulin-positive area to the total area of the tissue section as described previously (54–56).

Quantitation of VMAT2 transcript in pancreata of euglycemic and diabetic rats. Harvesting of pancreata for total RNA preparation was performed as follows: Anesthetized rats were opened with a midline incision, and the liver, stomach, and small intestine reflected to expose the pancreas. The abdominal cavity was then bathed with 5 ml of RNAlater from Ambion Inc. according to the manufacturer's recommendations. The head, body, and tail of the pancreas were dissected under RNAlater and removed to a 25-mm plastic Petri dish containing sufficient RNAlater to cover the excised tissue. The pancreas was cut into approximately 2-mm-thick sections, transferred to fresh RNAlater, and stored overnight at 4°C. Total pancreatic RNA was isolated and assessed for quality, and the specific transcript abundance was measured by real-time RT-PCR as previously described (28). The conditions used were as follows: 1 cycle at 95°C for

900 seconds, followed by 45 cycles of amplification (94°C for 15 seconds, 55°C for 20 seconds, and 72°C for 20 seconds). The oligonucleotides were synthesized by Invitrogen Corp. The primer sequences were as follows: 5′-TCATGAAGTGTGACGTTGACATCCGT-3′ (β-ACT-5′); 5′-CCTAGAAGCATTTGCGGTGCACGATG-3′ (β-ACT-3′); 5′-GCCCT-GCCCATCTGGATGAT-3′ (VMAT2-5′); 5′-CTTTGCAATAGCACCAC-CAGCAG-3′ (VMAT2-3′). The relative amounts of mRNA were calculated by the comparative cycle threshold method described by Livak and Schmittgen (57); the values were normalized by β-actin expression.

PET scan study protocol. Baseline PET scans were performed on 7-week-old male BB-DP rats. After the baseline scan, an additional 2 or 3 PET studies were performed through 12 weeks of age (Table 1). In later experiments, 2 additional PET scans were performed on 8-week-old or older BB-DP rats based on the presence of an abnormal glucose tolerance test. Before imaging, the animals were anesthetized with i.p. ketamine and xylazine. After a transmission scan of the area of interest had been acquired (for attenuation correction of the emission data), the radioligand [11C]DTBZ was administered (0.5–1.0 μCi/g) in saline as a bolus injection via the penile vein. PET scans of the animals were acquired dynamically from 0 to 60 minutes postinjection on a Concorde microPET R4 (CTI Molecular Imaging). The scanner provided a 100-by-80-mm field of view with a reconstructed resolution of 2.25 mm in the central 40 mm of the field of view. PET data were processed using an attenuation correction matrix obtained by the transmission scans; images were reconstructed using Fourier rebinning, followed by 2-dimensional, filtered back-projection using microPET manager software from CTI Molecular Imaging. Imaging of a male-baboon abdomen was performed as previously described (58) using [11C]DTBZ.

Data analysis and interpretation. Region of interest (ROI) analysis and image reconstruction were performed with ASIPro software from CTI Molecular Imaging. Visual analysis was performed by individuals experienced in PET interpretation using coronal, transverse, and sagittal reconstructions. Reconstructed PET images with a slice thickness of 5 mm were used to identify and measure radioligand activity within each organ of interest. ROIs were placed across image planes manually for the determination of time-activity curves. The ROIs were drawn using known landmarks, remaining [11C]DTBZ avidity in the pancreas of diabetic animals, and the baseline pattern of [11C]DTBZ uptake. One of these landmarks, the liver, is clearly visible in the reconstructed images as the site of [11C]DTBZ catabolism and excretion into bile (Figure 1). The kidneys are not shown in Figure 1 but were visible in early reconstructed images. The kidneys were used as additional landmarks. In normal animals, the renal cortex does not accumulate the radioligand and therefore provides a convenient negative con-trol for DTBZ uptake, as does the abdominal wall. Decay-corrected time-activity curves for [11C]DTBZ uptake in the ROIs were obtained from the tissues of interest (i.e., pancreas, right hepatic lobe and kidney, renal cortices, and the abdominal wall) and were based on sampling of approximately equal volumes (±10%) of tissue throughout the study. The comparison of pancreatic [11C]DTBZ uptake among all animals studied was performed by calculation of the max SUV for each animal at each time point studied. The max SUV was obtained from the highest activity measurement on the time-activity curve divided by injected dose of [11C]DTBZ normalized to the total body weight of the animal.

Statistics. The statistical significance of the associations among abnormal IPGTT, development of persistent hyperglycemia, and changes in the max SUV were analyzed by MedCalc software (version 8.1.1; MedCalc). Threshold values for changes in max SUV and AUC IPGTT in relation to the development of persistent hyperglycemia were determined using ROC curves calculated by Medicalc software (version 8.1.1). Both linear and nonlinear regression analysis was performed using NLREG software (http://www.nlreg.com). Paired measurements of AUC IPGTT and max SUV were fitted to the model equation AUC IPGTT = $b + c$/max SUV, where b and c are constants whose values were assigned by the regression software. The reported P value is the probability that the null hypothesis for the model is true, and that the constants b and c have a value of 0. P values less than 0.05 were considered statistically significant. Paired-sample testing for evaluation of the significance of changes in max SUV occurring during progression of diabetes within the population studied was performed using 2-tailed Student's t test.

Acknowledgments

Address correspondence to: Paul E. Harris, Department of Medicine, BB 20-06, Columbia University Medical Center, 650 West 168th Street, New York, New York 10032, USA. Phone: (212) 305-7363; Fax: (212) 305-7348; E-mail: peh1@columbia.edu.

1. Franke, B., Galloway, T.S., and Wilkin, T.J. 2005. Developments in the prediction of type 1 diabetes mellitus, with special reference to insulin autoantibodies. *Diabetes Metab. Res. Rev.* **21**:395–415.
2. Bernard-Kargar, C., and Ktorza, A. 2001. Endocrine pancreas plasticity under physiological and pathological conditions. *Diabetes.* **50**(Suppl. 1):S30–S35.
3. Weir, G.C., Bonner-Weir, S., and Leahy, J.L. 1990. Islet mass and function in diabetes and transplantation. *Diabetes.* **39**:401–405.
4. Sreenan, S., et al. 1999. Increased beta-cell proliferation and reduced mass before diabetes onset in the nonobese diabetic mouse. *Diabetes.* **48**:989–996.
5. Larsen, M.O., et al. 2003. Loss of beta-cell mass leads to a reduction of pulse mass with normal periodicity, regularity and entrainment of pulsatile insulin secretion in Gottingen minipigs. *Diabetologia.* **46**:195–202.
6. Kjems, L.L., et al. 2001. Decrease in beta-cell mass leads to impaired pulsatile insulin secretion, reduced postprandial hepatic insulin clearance, and relative hyperglucagonemia in the minipig.

Diabetes. **50**:2001–2012.
7. Larsen, M.O., Rolin, B., Wilken, M., Carr, R.D., and Gotfredsen, C.F. 2003. Measurements of insulin secretory capacity and glucose tolerance to predict pancreatic beta-cell mass in vivo in the nicotinamide/streptozotocin Gottingen minipig, a model of moderate insulin deficiency and diabetes. *Diabetes.* **52**:118–123.
8. McCulloch, D.K., Koerker, D.J., Kahn, S.E., Bonner-Weir, S., and Palmer, J.P. 1991. Correlations of in vivo beta-cell function tests with beta-cell mass and pancreatic insulin content in streptozocin-administered baboons. *Diabetes.* **40**:673–679.
9. Gepts, W. 1965. Pathologic anatomy of the pancreas in juvenile diabetes mellitus. *Diabetes.* **14**:619–633.
10. Gepts, W., and Lecompte, P.M. 1981. The pancreatic islets in diabetes. *Am. J. Med.* **70**:105–115.
11. Saito, K., Yaginuma, N., and Takahashi, T. 1979. Differential volumetry of A, B and D cells in the pancreatic islets of diabetic and nondiabetic subjects. *Tohoku J. Exp. Med.* **129**:273–283.
12. Bonner-Weir, S., Trent, D.F., and Weir, G.C. 1983.

Partial pancreatectomy in the rat and subsequent defect in glucose-induced insulin release. *J. Clin. Invest.* **71**:1544–1553.
13. Tominaga, M., Maruyama, H., Bolli, G., Helderman, J.H., and Unger, R.H. 1986. Simulation of the normal glucopenia-induced decline in insulin partially restores the glucagon response to glucopenia in isolated perfused pancreata of streptozotocin-diabetic rats. *Endocrinology.* **118**:886–887.
14. Clark, P.B., et al. 2003. Neurofunctional imaging of the pancreas utilizing the cholinergic PET radioligand [(18)F]4-fluorobenzyltrozamicol. *Eur. J. Nucl. Med. Mol. Imaging.* **31**:258–260.
15. Seltzer, M.A., et al. 2004. Radiation dose estimates in humans for (11)C-acetate whole-body PET. *J. Nucl. Med.* **45**:1233–1236.
16. Shreve, P.D., and Gross, M.D. 1997. Imaging of the pancreas and related diseases with PET carbon-11-acetate. *J. Nucl. Med.* **38**:1305–1310.
17. Markmann, J.F., et al. 2003. Magnetic resonance-defined periportal steatosis following intraportal islet transplantation: a functional footprint of islet

graft survival? *Diabetes.* **52**:1591–1594.

18. Moore, A., Bonner-Weir, S., and Weissleder, R. 2001. Noninvasive in vivo measurement of beta-cell mass in mouse model of diabetes. *Diabetes.* **50**:2231–2236.

19. Ladriere, L., Malaisse-Lagae, F., Alejandro, R., and Malaisse, W.J. 2001. Pancreatic fate of a (125)I-labelled mouse monoclonal antibody directed against pancreatic B-cell surface ganglioside(s) in control and diabetic rats. *Cell Biochem. Funct.* **19**:107–115.

20. Malaisse, W.J., Ladriere, L., and Sener, A. 2000. Pancreatic fate of 6-deoxy-6-[125I]iodo-D-glucose: in vitro experiments. *Endocrine.* **13**:89–94.

21. Malaisse, W.J., Doherty, M., Ladriere, L., and Malaisse-Lagae, F. 2001. Pancreatic uptake of [2-(14C)alloxan. *Int. J. Mol. Med.* **7**:311–315.

22. Garnuszek, P., et al. 2000. Identification of transplanted pancreatic islet cells by radioactive dithizone-[131I]-histamine conjugate. Preliminary report. *Nucl. Med. Rev. Cent. East. Eur.* **3**:61–63.

23. Ladriere, L., Malaisse-Lagae, F., and Malaisse, W.J. 2000. Uptake of tritiated glibenclamide by endocrine and exocrine pancreas. *Endocrine.* **13**:133–136.

24. Sweet, I.R., et al. 2004. Systematic screening of potential beta-cell imaging agents. *Biochem. Biophys. Res. Commun.* **314**:976–983.

25. Atouf, F., Czernichow, P., and Scharfmann, R. 1997. Expression of neuronal traits in pancreatic beta cells. Implication of neuron-restrictive silencing factor/repressor element silencing transcription factor, a neuron-restrictive silencer. *J. Biol. Chem.* **272**:1929–1934.

26. Bernal-Mizrachi, E., Cras-Meneur, C., Ohsugi, M., and Permutt, M.A. 2003. Gene expression profiling in islet biology and diabetes research. *Diabetes Metab. Res. Rev.* **19**:32–42.

27. Scharfmann, R., and Czernichow, P. 1996. Differentiation and growth of pancreatic beta cells. *Diabetes Metab.* **22**:223–228.

28. Maffei, A., et al. 2004. Identification of tissue-restricted transcripts in human islets. *Endocrinology.* **145**:4513–4521.

29. Vander Borght, T.M., et al. 1995. In vivo imaging of the brain vesicular monoamine transporter. *J. Nucl. Med.* **36**:2252–2667.

30. Anlauf, M., et al. 2003. Expression of the two isoforms of the vesicular monoamine transporter (VMAT1 and VMAT2) in the endocrine pancreas and pancreatic endocrine tumors. *J. Histochem. Cytochem.* **51**:1027–1040.

31. Weihe, E., and Eiden, L.E. 2000. Chemical neuroanatomy of the vesicular amine transporters. *FASEB J.* **14**:2435–2449.

32. Weihe, E., Schafer, M.K., Erickson, J.D., and Eiden, L.E. 1994. Localization of vesicular monoamine transporter isoforms (VMAT1 and VMAT2) to endocrine cells and neurons in rat. *J. Mol. Neurosci.* **5**:149–164.

33. Ramanathan, S., and Poussier, P. 2001. BB rat lyp mutation and type 1 diabetes. *Immunol. Rev.* **184**:161–171.

34. Polychronakos, C. 2004. Animal models of spontaneous autoimmune diabetes: notes on their relevance to the human disease. *Curr. Diab. Rep.* **4**:151–154.

35. Rossini, A.A., Mordes, J.P., and Like, A.A. 1985. Immunology of insulin-dependent diabetes mellitus. *Annu. Rev. Immunol.* **3**:289–320.

36. DaSilva, J.N., Carey, J.E., Sherman, P.S., Pisani, T.J., and Kilbourn, M.R. 1994. Characterization of [11C]tetrabenazine as an in vivo radioligand for the vesicular monoamine transporter. *Nucl. Med. Biol.* **21**:151–156.

37. Scherman, D. 1986. Dihydrotetrabenazine binding and monoamine uptake in mouse brain regions. *J. Neurochem.* **47**:331–339.

38. Scherman, D., Jaudon, P., and Henry, J.P. 1983. Characterization of the monoamine carrier of chromaffin granule membrane by binding of [2-3H]dihydrotetrabenazine. *Proc. Natl. Acad. Sci. U. S. A.* **80**:584–588.

39. Henry, J.P., Sagne, C., Bedet, C., and Gasnier, B. 1998. The vesicular monoamine transporter: from chromaffin granule to brain. *Neurochem. Int.* **32**:227–246.

40. Tomita, T., and Doull, V. 1992. Correlation of morphometric analysis of pancreatic islets and diabetes in spontaneously diabetic BB/W rats. *Diabetes Res.* **19**:49–58.

41. Mei, Q., Mundinger, T.O., Lernmark, A., and Taborsky, G.J., Jr. 2002. Early, selective, and marked loss of sympathetic nerves from the islets of BioBreeder diabetic rats. *Diabetes.* **51**:2997–3002.

42. Lundquist, I., Ahren, B., Hansson, C., and Hakanson, R. 1989. Monoamines in pancreatic islets of guinea pig, hamster, rat, and mouse determined by high performance liquid chromatography. *Pancreas.* **4**:662–667.

43. Iturriza, F.C., and Thibault, J. 1993. Immunohistochemical investigation of tyrosine-hydroxylase in the islets of Langerhans of adult mice, rats and guinea pigs. *Neuroendocrinology.* **57**:476–480.

44. Ishihara, H., Maechler, P., Gjinovci, A., Herrera, P.L., and Wollheim, C.B. 2003. Islet beta-cell secretion determines glucagon release from neighbouring alpha-cells. *Nat. Cell Biol.* **5**:330–335.

45. Satin, L.S., and Kinard, T.A. 1998. Neurotransmitters and their receptors in the islets of Langerhans of the pancreas: what messages do acetylcholine, glutamate, and GABA transmit? *Endocrine.* **8**:213–223.

46. Sharp, G.W., et al. 1975. Studies on the mechanism of insulin release. *Fed. Proc.* **34**:1537–1548.

47. Ste Marie, L., and Palmiter, R.D. 2003. Norepinephrine and epinephrine-deficient mice are hyperinsulinemic and have lower blood glucose. *Endocrinology.* **144**:4427–4432.

48. Kilbourn, M.R. 1997. In vivo radiotracers for vesicular neurotransmitter transporters. *Nucl. Med. Biol.* **24**:615–619.

49. Koeppe, R.A., et al. 2005. 11C-DTBZ and 18F-FDG PET measures in differentiating dementias. *J. Nucl. Med.* **46**:936–944.

50. Kumar, A., et al. 2003. [11C]DTBZ-PET correlates of levodopa responses in asymmetric Parkinson's disease. *Brain.* **126**:2648–2655.

51. Jewett, D.M., Kilbourn, M.R., and Lee, L.C. 1997. A simple synthesis of [11C]dihydrotetrabenazine (DTBZ). *Nucl. Med. Biol.* **24**:197–199.

52. Kilbourn, M.R., Lee, L.C., Heeg, M.J., and Jewett, D.M. 1997. Absolute configuration of (+)-alpha-dihydrotetrabenazine, an active metabolite of tetrabenazine. *Chirality.* **9**:59–62.

53. Weksler-Zangen, S., et al. 2001. The newly inbred cohen diabetic rat: a nonobese normolipidemic genetic model of diet-induced type 2 diabetes expressing sex differences. *Diabetes.* **50**:2521–2529.

54. Garofano, A., Czernichow, P., and Breant, B. 2000. Impaired beta-cell regeneration in perinatally malnourished rats: a study with STZ. *FASEB J.* **14**:2611–2617.

55. Butler, A.E., et al. 2003. Beta-cell deficit and increased beta-cell apoptosis in humans with type 2 diabetes. *Diabetes.* **52**:102–110.

56. Paris, M., Bernard-Kargar, C., Berthault, M.F., Bouwens, L., and Ktorza, A. 2003. Specific and combined effects of insulin and glucose on functional pancreatic beta-cell mass in vivo in adult rats. *Endocrinology.* **144**:2717–2727.

57. Livak, K.J., and Schmittgen, T.D. 2001. Analysis of relative gene expression data using real-time quantitative PCR and the $2^{-\Delta\Delta C_T}$ method. *Methods.* **25**:402–408.

58. Kumar, J.S., et al. 2006. Synthesis and in vivo validation of [O-methyl-11C]2-{4-[4-(7-methoxynaphthalen-1-yl)piperazin- 1-yl]butyl}-4-methyl-2H-[1,2,4]triazine-3,5-dione: a novel 5-HT1A receptor agonist positron emission tomography ligand. *J. Med. Chem.* **49**:125–134.